Relativistic nonlinear Thomson scattering as attosecond x-ray source

K. Lee and Y. H. Cha

Laboratory for Quantum Optics, Korea Atomic Energy Research Institute, P. O. Box 105, Deokjin-Dong, Yuseong-Gu, Daejeon 305-600, Korea

M. S. Shin, B. H. Kim, and D. Kim

Physics Department, Pohang University of Science and Technology, San 31 Hyoja-Dong, Nam Ku, Pohang, Kyungbuk 790-784, Korea

Relativistic, nonlinear Thomson scattering by an electron of an intense laser field has been investigated by computer simulation. Under a laser field with a pulse duration of 20-fs full width at half maximum and an intensity of 10^{20} W/cm^2, the motion of an electron is highly relativistic and generates an ultrashort radiation of 2 as with photon energies from 100 to 600 eV. An interesting modulated structure of the spectrum is observed and analyzed. A radiation produced by the zigzag motion of an electron under a linearly polarized laser has better characteristics than by a helical motion under a circularly polarized laser pulse in terms of an angular divergence and an energy spectrum. The effect of ion field in a plasma was also investigated, which shows that for a laser intensity of 10^{20} W/cm^2, the ion field due to an ion density of up to 7×10^{18} cm^{-3} can be ignored during the laser pulse.

I. INTRODUCTION

The advent of the CPA (chirped pulse amplification) lasers [1] has allowed researchers to be interested in the high field-matter interaction both for fundamental study and applications. The ultrashort intense laser technology [2] has opened up a new branch of research such as relativistic plasma physics. The generation of subfemtosecond pulse is considered as one of the most important potential applications in this branch of research. Such ultrashort pulses are useful to explore the new regime of dynamics such as electron dynamics in an atom and strong nuclear interactions. Various schemes have been explored for the generation of subfemtosecond pulse in the visible range. The schemes utilize Fourier synthesis [3,4], a strongly driven classical oscillator in a Coulomb potential [5], the use of two short perpendicularly polarized pulses [6], high-order harmonics from a nonlinear medium under an ultrafast intense laser [7,8], stimulated Raman scattering [9–12], and molecular coherence driven by electromagnetically induced transparency [13,14].

In an extreme ultraviolet range, the train of 250 as pulse with a few 10 eV photon energy has been experimentally demonstrated [15,16] and Hentschel *et al.* [17] observed a 650 as Gaussian pulse at 90 eV photon energy in a higher-order harmonics generation experiment. The direct irradiation of an intense laser on a target produces a pulse whose pulse duration is limited by the atomic transition rate. Inner-shell atomic states, which have fast Coster-Kronig decay process were investigated, are expected to produce a femtosecond x-ray laser pulse [18]. Several schemes using a scattering process of an intense laser pulse by free electrons have been explored: the relativistic Doppler shift which arises from the backscattering of a laser radiation from a counter-streaming relativistic electron beam [19–21] and the harmonic frequency upshift [20]. The first one is referred to as Compton backscattering and the other as relativistic nonlinear Thomson scattering.

The harmonic spectrum of the relativistic nonlinear Thomson scattering by a single electron has been investigated in an analytical way [22–25]. Recently, such a prediction has been experimentally verified by observing the angular patterns of the harmonics for a relatively low laser intensity of 4.4×10^{18} W/cm^2 [26,27]. Esarey *et al.* [20] has investigated the plasma effect on the nonlinear Thomson scattering and presented a set of the parameters for generating a 9.4-ps x-ray pulse with a high peak flux of 6.5×10^{21} photons/s at 310 eV photon energy using an ultrahigh laser intensity of 10^{20} W/cm^2. Ueshima *et al.* [28] has suggested several methods to enhance the radiation power, using particle-in-cell simulations even for a higher intensity. Kaplan and Shkolnikov *et al.* [29] proposed a scheme for the generation of zeptosecond (10^{-21} sec) radiation using two counter-propagating circularly polarized lasers, named as lasertron.

In this paper, we present the angular, spectral distribution, and the power in detail of the radiation by a single electron irradiated by a 20 fs FWHM (full width at half maximum) laser pulse. The results show that with a laser intensity of 10^{20} W/cm^2, ultrashort pulses of 2-as radiation with a photon energy from 100 eV up to 600 eV can be generated. The modulated structure of the energy spectrum will be presented and analyzed. Considering the radiation power and the angular distribution, the radiation under a linearly polarized driving laser has better characteristics than under a circularly polarized driving laser.

II. FORMULATION

The motion of a single electron in a high intensity laser field is described by the following relativistic equation of motion:

$$m_e \frac{d}{dt'}(\gamma \vec{v}) = -e(\vec{E} + \vec{\beta} \times \vec{B}), \tag{1}$$
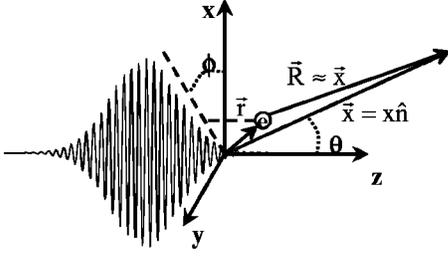
FIG. 1. Geometry for the propagation of an incident driving laser and the radiation by an accelerated electron.

where m_e is the electron mass, $\vec{v}$ the velocity of the electron, $\gamma = 1/\sqrt{1-\beta^2}$ the relativistic factor, $\vec{\beta} = \vec{v}/c$, and $\vec{E}$ and $\vec{B}$ are the electric and magnetic field of an incident laser, respectively, which can be expressed as

$$\vec{E} = \frac{E_o}{\sqrt{2}} f(t) [\sqrt{1+p} \, \cos(\vec{k} \cdot \vec{r} - \omega_L t') \hat{x}$$
$$+ \sqrt{1-p} \, \sin(\vec{k} \cdot \vec{r} - \omega_L t') \hat{y}], \tag{2}$$

$$\vec{B} = \hat{k} \times \vec{E}, \tag{3}$$

where E_0 is a peak electric field strength, $f(t)$ an envelope function, and $\vec{k}$ the wave vector. The polarization is described by the parameter p: 1 for a linear and 0 for a circular polarization. Assuming that the envelope function varies slowly, the motion of the initially stationary electron is given as follows [20]:

$$\vec{\beta}_\perp = \frac{2\vec{a}}{a^2+2}, \tag{4}$$

$$\beta_z = \frac{a^2}{a^2+2}, \tag{5}$$

$$\gamma = 1 + \frac{a^2}{2}, \tag{6}$$

where the field strength parameter a is given by

$$a = \frac{eE}{m_e c \omega_L} \tag{7}$$

$$= 8.5 \times 10^{-10} [\lambda_L(\mu m)] \sqrt{I(\text{W/cm}^2)}. \tag{8}$$

The above equations show that at a high laser intensity ($a > 1$ or $I > [\lambda_L^{-2}(\mu m)] 1.4 \times 10^{18}$ W/cm^2), the electron's motion becomes highly relativistic or nonlinear, which generates the harmonics.

The angular distribution of the radiated power [30] detected far away from the electron toward the direction $\hat{n}$ [Fig. 1] at a time t is then calculated as

$$\frac{dP(t)}{d\Omega} = |A(t)|^2, \tag{9}$$
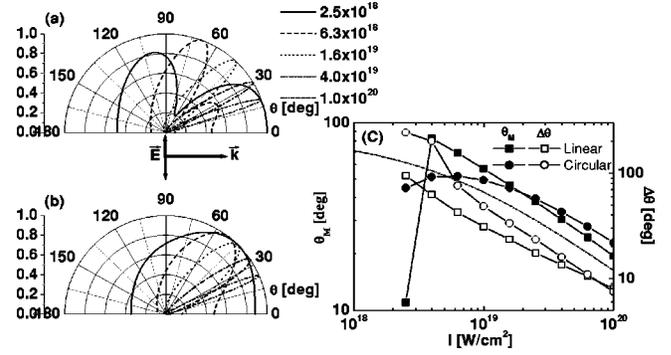
FIG. 2. Angular distributions at $\phi = 0°$ of the time-integrated radiated power for various laser intensities: (a) a linearly and (b) a circularly polarized laser. For comparison, the radiations are normalized to their own maxima. The angle θ_M at which the radiation becomes maximum and its angular divergence $\Delta\theta$ are plotted in (c), wherein the dash-dotted line is the estimated θ_M by Eq. (15).

$$A(t) = \sqrt{\frac{e^2}{4\pi c}} \left[\frac{\hat{n} \times \{(\hat{n}-\vec{\beta}) \times \dot{\vec{\beta}}\}}{(1-\vec{\beta}\cdot\hat{n})^3} \right]_{t'}, \tag{10}$$

where t' is the electron's time or retarded time and related to t by

$$t = t' + \frac{x - \hat{n} \cdot \vec{r}(t')}{c}. \tag{11}$$

Then the angular spectral intensity can be obtained by the Fourier transform of $A(t)$ as

$$\frac{d^2 I}{d\omega d\Omega} = 2|A(\omega)|^2, \tag{12}$$

$$A(\omega) = \frac{1}{\sqrt{2\pi}} \int_{-\infty}^{\infty} A(t) e^{-i\omega t} dt. \tag{13}$$

III. RESULTS AND DISCUSSIONS

Radiation characteristics are investigated for various laser peak intensities (I) and for two different polarizations. A driving laser has a Gaussian envelope with a pulse duration of 20-fs FWHM and the central wavelength at 800 nm. This is a typical pulse shape from Ti:sapphire CPA lasers.

The quivering amplitude of an electron at $I = 10^{20}$ W/cm^2 amounts to about 0.9 μm. This is still quite small compared to a typical focal spot size (order of a few ten micrometers) of a laser light so that the plane wave approximation is valid and adopted for this radiation calculation.

The time-integrated angular (θ) distribution of the radiated power at $\phi = 0°$ are plotted in Figs. 2(a) and 2(b) for linearly and circularly polarized driving lasers, respectively. In Fig. 2, each radiation is normalized to its maximum for easy comparison of the angular distributions between different laser intensities. As the laser intensity increases, the radiation is directed toward the z axis with a narrower diver-

gence. Regardless of the laser polarization, the increase of a laser intensity enhances not only a total radiated power but also a radiation flux. This characteristic makes the radiation by relativistic nonlinear Thomson scattering interesting as a radiation source. Well-defined radiation has been proven to be useful in many applications.

The polar angle θ_M, at which the radiation reaches its maximum is plotted in Fig. 2(c). At low laser intensities (2×10^{18} W/cm^2 or less), even though the electron takes a relativistic motion, the angular distribution of the radiation does not deviate much from that of the dipole radiation. Even though there are harmonic radiations, the θ_M lies near the z axis. One interesting feature in the angular distribution for the case of a linear polarization is that at low intensities, there are two significant peaks: one directed toward the z axis and the other toward the electron's velocity. The peak in the z axis is due to the dipole radiation and the other is caused by the relativistic motion. One can notice that as the laser intensity increases, the dipole component decreases but the nonlinear component increases. At a laser intensity of 6.3×10^{18} W/cm^2, the nonlinear component is already larger than the dipole component. Such a transition occurs in the narrower range of the laser intensity for the case of a linear polarization than for the case of a circular polarization. This is caused by the difference in the spectra of the radiations for the two cases. The spectrum for a linear polarization has higher-energy photons than for a circularly polarization, which means that for the same laser intensity, the linearly polarized laser makes the motion of an electron more relativistic. Higher-energy photons produced by the nonlinear or relativistic motion of an electron are directed toward the electron's velocity. For a highly relativistic electron, since the radiation is directed toward its velocity, θ_M can be simply estimated as

$$\tan \theta_M \simeq \frac{\beta_x}{\beta_z}, \tag{14}$$

$$= \frac{2}{a}, \tag{15}$$

where Eqs. (4) and (5) are used for Eq. (15). The above simple estimation for different peak intensities are compared with the simulation in Fig. 2(c). Note that θ_M is still large even for $I = 10^{20}$ W/cm^2. The direction of the emitted radiation is off the direction of the driving laser,which is a useful aspect in terms of application, unlike in the high harmonics generated by lower-power femtosecond lasers.

Figure 3 is the azimuthal(ϕ) angular distribution of the radiated power under $I = 10^{20}$ W/cm^2 for the case of a linear polarization [Fig. 3(a)] and for the case of a circular polarization [Fig. 3(b)]. In the azimuthal angle ϕ, the radiations are directed toward the direction of the laser electric field, which are $\phi = 0°$, and $180°$ for the case of a linear polarization, and symmetric for the case of a circular polarization.

The time history of the radiated power per solid angle at the direction of $\theta = \theta_M$ and $\phi = 0°$ are plotted in Figs. 4(a) and 4(b) for the case of a linear and a circular polarization, respectively. The spikelike radiations with almost constant
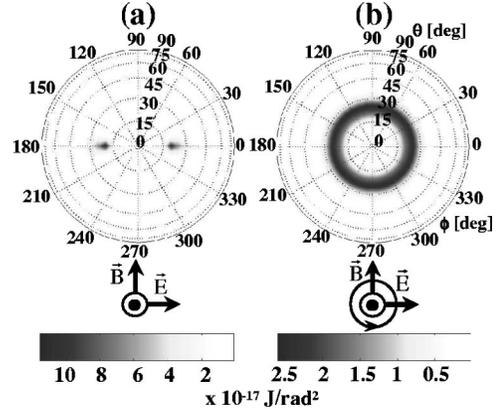
FIG. 3. The contour of the angular distribution of the radiation under $I = 10^{20}$ W/cm^2 for the cases of (a) a linearly and (b) a circularly polarized laser. The directions of laser fields are shown below the figures and the laser pulse propagates out of the page.

intervals are produced. This interval is related to the oscillation period of the driving laser, but the effect of the retarded time and the relativistic motion of an electron makes not only the interval different from the laser's oscillation period but also the intervals between the peaks different from each other. These are manifested as a modulation in the spectrum (Fig. 5) as discussed later.

The highest peaks are magnified in order to observe the pulse shapes for the cases of linearly [Fig. 4(c)] and circularly [Fig. 4(d)] polarized driving lasers. The estimated FWHM of the radiation pulse duration are 2.0 as and 2.2 as for a linearly and circularly polarized laser, respectively. One interesting thing is that there are two pulses with an interval of 21 as for a linearly polarized laser; while a single pulse appears for a circularly polarized laser. The single pulse during a single cycle of the driving laser in the case of a circular polarization can be easily understood by considering the circular motion (more accurately a helical motion) of an electron. The double-pulse structure in the case of a linearly polarized laser can be understood by considering the dynamics and a time difference between an electron's own time t' and a detector's time t in Eq. (11). During a half cycle of the driving laser(that is, the electron moving toward $\theta = \theta_M$ and $\phi = 0°$), the double pulse is produced by the disappearance of $\dot{\vec{\beta}}$ in the mean time, where there is no radiation. Thus, with a low but relativistic intensity ($I = 10^{18}$ W/cm^2) driving laser, the double pulse appears with an interval of the quarter cycle of the laser. As the intensity gets higher, the highly relativistic effect reduces the time interval as

$$\frac{\Delta t}{\Delta t'} \simeq 1 - \hat{n} \cdot \vec{\beta}, \tag{16}$$

which comes from Eq. (11). In the above equation, $\Delta t'$ is the time interval in which the electron emits radiations and Δt is the time interval in which a detector receives the radiations. For the direction of the electron's velocity, using the solutions of β's for $a \gg 1$, the following relation is obtained:
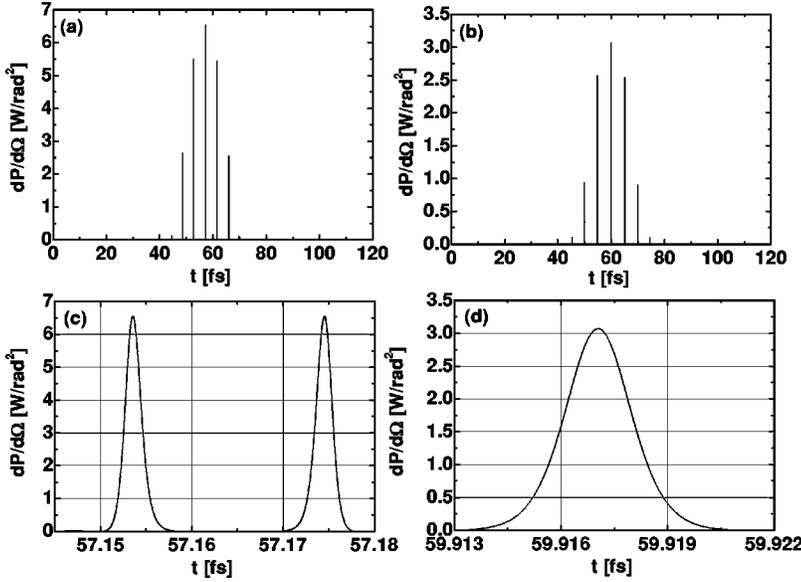
FIG. 4. The time history of the radiated power for $I = 10^{20}$ W/cm^2 at the direction of maximum radiation (see Fig. 2) for (a) a linearly and (b) a circularly polarized laser. To investigate the pulse shape, each pulse is magnified for (c) a linearly and (d) a circularly polarized laser.

$$\frac{\Delta t}{\Delta t'} \simeq \frac{2}{a^4}. \qquad (17)$$

Since the propagation velocity β_z of an electron approaches to c for an ultrahigh intensity laser, $\Delta t'$ can be described as

$$\Delta t' \simeq \frac{T_L}{4} \gamma, \qquad (18)$$

$$\simeq \frac{T_L}{4} \frac{a^2}{2}. \qquad (19)$$

This shows that $\Delta t'$ becomes larger than the quarter cycle ($T_L/4$) of the laser frequency for a higher intensity of laser. For $I = 10^{20}$ W/cm^2 ($a = 6.8$), Eq. (17), with the help of Eq. (19), estimates the pulse interval as 14.6 as.

With respect to the pulse width, we consider the time interval during which the acceleration is the largest because the radiated power is proportional to the square of the acceleration. For the linearly polarized driving laser, the acceleration is the largest, concentrated at high intensities, and especially at the turning points of the zigzag motion of an electron. Since the quiver amplitude of the electron is $a\lambda_L$, the geometrical length during which the electron emits the radiation is roughly $a\lambda_L\Delta\theta$, where $\Delta\theta$ is the angular divergence of the radiation. Hence, the time duration of the radiation is

$$\Delta t' \simeq a\Delta\theta \frac{\lambda_L}{c}. \qquad (20)$$

For $I = 10^{20}$ W/cm^2 ($a = 6.8$) and $\Delta\theta = 8°$ [Fig. 2(c)], $\Delta t = 2.3$ as, which is the same as the simulation result and two orders of magnitude shorter than recent results obtained in the higher-order harmonic experiments [15–17].

For a laser intensity of $I = 10^{20}$ W/cm^2, the angular spectral intensity (spectral intensity per solid angle) at the direction of $\theta = \theta_M$ and $\phi = 0°$ are plotted in Fig. 5 for the case of a linear polarization [Fig. 5(a)] and for a circular polarization [Fig. 5(b)]. First of all, a large fraction of high-energy photons from 100 eV up to 600 eV are generated due to the relativistic motion of an electron. More higher-energy photons are generated in the case of a linear polarization than in the case of a circular polarization because of a higher instantaneous acceleration in the case of a linear polarization. It is interesting to notice that there are bunched or modulated structures in the spectrum. First, the modulations with an interval of about 25 eV appear for both polarizations. For the linear polarization, another modulation with an interval of about 200 eV is observed. The small-interval modulation that appears for both polarizations is caused by the slight difference in the time interval of the radiation peaks [Figs. 4(a) and 4(b)]. For the case of the linear polarization, the time interval between the second-highest and third-highest peak is 4.27 fs and that between the first-highest and second-highest peak is 4.43 fs, the difference of which is 0.16 fs, which
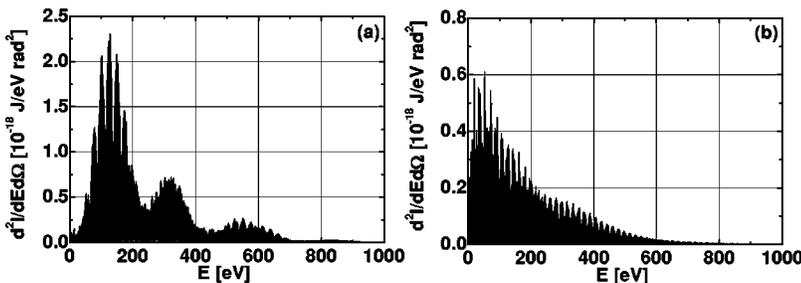
FIG. 5. The spectral intensity for $I = 10^{20}$ W/cm^2 at the direction of a maximum radiation (see Fig. 2) for (a) a linearly and (b) a circularly polarized laser.
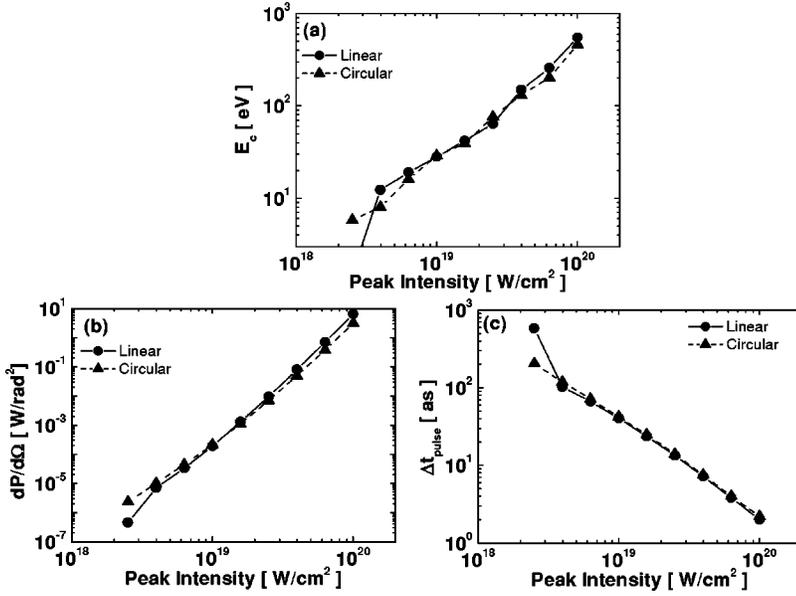
FIG. 6. The dependence on the laser intensities of the radiation characteristics: (a) critical photon energy E_c at which the spectral intensity reduces to one-tenth of its maximum, (b) angular power, and (c) FWHM of the pulse duration of the highest peaks. All data are taken at the direction of the maximum radiation.

corresponds to about 25 eV in the energy scale. The large-interval modulation in the case of the linear polarization, which does not appear in the case of the circular polarization, is caused by the double-peak structure of the radiation [Fig. 4(c)], with an interval of about 20 as which corresponds to about 200 eV in the energy scale.

The variations of the critical photon energy E_c at which the angular spectral intensity has one-tenth of its maximum, and the angular power and the pulse width with respect to the laser intensities are plotted in Fig. 6. The scalings to the laser intensity are estimated approximately as

$$E_c \propto I^{1.5}, \tag{21}$$

$$\frac{dP}{d\Omega} \propto I^{4.7}, \tag{22}$$

$$\Delta t_{FWHM} \propto I^{-1.4}. \tag{23}$$

The field by a nearby ion in a high density plasma can affect the dynamics of an oscillating electron. This effect leads to the generation of Bremsstrahlung radiation. A critical density n_c, below which the effect of the ion field can be ignored, is simply estimated considering the effect by ion microfields accumulated during the motion of an electron for an laser pulse. Even though an ion field at a position is negligible compared to the laser field, the disturbance by ion fields accumulated during the motion of an electron may result in the distortion of the oscillatory motion of an electron. The maximal effect by ion fields exerted on the motion of an electron is estimated as an average ion field multiplied by the number of ions encountered. This yields the lower limit of an electron density, critical density, above which the effect from the distortion of the oscillatory motion of electrons begins to be important. The calculation of the exact ion microfield demands the knowledge of ion microfield distribution, which is out of the scope of this paper. As an approximation to estimate the order of the critical density, here we use Holtsmark's normal strength [31]

$$F_0 = 2\pi \left(\frac{4}{15}\right)^{2/3} zen^{2/3}, \tag{24}$$

where z is the ion charge number, e the electronic charge, and n the ion density. F_0 represents, within a factor, the most probable field strength for a given distribution of ions with a density n. This serves us to estimate the order of the critical density. The number of ions encountered is estimated to be the number of ions in an effective volume surrounding the electron path, the radius of whose cross section is r_{mean}, the mean distance between ions and the length l_{path} is the total path length of an electron during the laser pulse. The ion density and r_{mean} are related by $3/(4\pi r_{mean}^3) = n$. Then the maximally accumulated ion field effect amounts to the following E_{ion}^{acc}:

$$E_{ion}^{acc} \simeq 2\pi \left(\frac{4}{15}\right)^{2/3} zen^{2/3} n\pi r_{mean}^2 l_{path}. \tag{25}$$

This could be compared with the electric field strength of a driving laser, E_L, multiplied by a measuring factor for the degree of perturbation, α. This gives the following estimation of the critical density:

$$n_c \ (\text{cm}^{-3}) \simeq 6.1 \times 10^7 \frac{\alpha}{z} \frac{\sqrt{I \ (\text{W/cm}^2)}}{l_{path} \ (\text{cm})}. \tag{26}$$

The above equation is plotted in Fig. 7 with $\alpha = 0.1$ and $z = 1$, where l_{path} is obtained by the numerical integration of the electron's motion. The decrease of the critical density with increasing the laser intensity is caused by a rapid increase of l_{path} due to a highly relativistic motion along the direction of a laser propagation. For a hydrogen plasma ($z = 1$) and $\alpha = 0.1$, the above estimation gives $n_c \sim 7 \times 10^{18}$ cm^{-3} for $I = 10^{20}$ W/cm^2. This agrees well with an estimation using particle-in-cell simulation [28]. This estimation shows that the effect of the ion field during the laser oscillation seems quite negligible up to a rather high density.
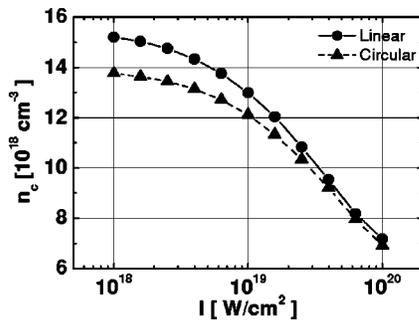
FIG. 7. Estimated critical densities below which the effect of ion field can be neglected are plotted for the case of $\alpha = 0.1$ and $z = 1$.

However, bremsstrahlung radiation from a high density plasma after the laser pulse will be significant in real experiments. The experimental observation of Larmor radiation in relativistic regime requires a target design, which minimizes the bremsstrahlung radiation, or a time resolved detection in ultrafast time scale.

At this density, the incoherent addition of the radiations from individual electrons in a cylinder of 10 μm diameter and 10 μm length by the nonlinear, relativistic Thomson scattering of a linearly polarized laser of 10^{20} W/cm² can produce the power intensity of 3.5×10^8 W/cm², 10 cm away from the source. This corresponds to the total photon number of 2.3×10^8 photons/s on an area of 1.4×1.4 cm². Since the radiation generated by the linearly polarized laser has the narrower angular distribution, higher-energy photon spectrum and higher power than by the circularly polarized laser, the radiation by the linearly polarized laser will be more useful as a high intensity x-ray radiation source.

IV. SUMMARY

The relativistic, nonlinear scattering of a high intensity laser by a single electron has been investigated numerically. For an ultraintense laser intensity of 10^{20} W/cm², the scattered radiation has a narrow angular divergence of 8° with the photon energy up to 600 eV. The investigation shows that this mechanism has a potential to produce an ultrashort pulse in the attosecond time scale. The characteristic temporal variation of radiation generates an interesting modulated energy spectrum, which is caused by the double-peak structure for the linear polarization and by the difference in the time interval between the radiation peaks for both of the polarizations.

The ion field during the laser oscillation is expected to be negligible up to a plasma density of 7×10^{18} cm⁻³. In this plasma density, the relativistic Thomson scattering with a laser of 10^{20} W/cm² generates x-ray photons up to 600 eV with the flux of 1.2×10^8 photons/s cm².

Further, investigations are still required to include the effect of multielectrons; that is, electrons at different z positions emit radiations with time interval in electrons' view. The phase matching of the radiations from different electrons needs to be addressed.

[1] M.D. Perry and G. Mourou, Science **264**, 917 (1994).

[2] G.A. Mourou, C.P.J. Barty, and M.D. Perry, Phys. Today **51**, 22 (1998).

[3] T.W. Hansch, Opt. Commun. **80**, 71 (1990).

[4] Gy. Farkas and Cs. Toth, Phys. Lett. A **168**, 447 (1992).

[5] S.E. Harris, J.J. Macklin, and T.W. Hansch, Opt. Commun. **100**, 487 (1993).

[6] P.B. Corkum, N.H. Burnett, and M.Y. Ivanov, Opt. Lett. **19**, 1870 (1994).

[7] K.J. Schafer and K.C. Kulander, Phys. Rev. Lett. **78**, 638 (1997).

[8] I.P. Christov, M.M. Murnane, and H.C. Kapteyn, Phys. Rev. Lett. **78**, 1251 (1997).

[9] A.E. Kaplan, Phys. Rev. Lett. **73**, 1243 (1994).

[10] S. Yoshikawa and T. Imasaka, Opt. Commun. **96**, 94 (1993).

[11] A.E. Kaplan and P.L. Shkolnikov, J. Opt. Soc. Am. B **13**, 347 (1996).

[12] H. Kawano, Y. Hirakawa, and T. Imasaka, IEEE J. Quantum Electron. **34**, 260 (1998).

[13] S.E. Harris and A.V. Sokolov, Phys. Rev. Lett. **81**, 2894 (1998).

[14] Fam Le Kien, J.Q. Liang, M. Katsuragawa, K. Ohtsuki, K. Hakuta, and A.V. Sokolov, Phys. Rev. A **60**, 1562 (1999).

[15] P.M. Paul, E.S. Toma, P. Breger, G. Mullot, F. Auge, Ph. Balcou, H.G. Muller, and P. Agostini, Science **292**, 1689 (2001).

[16] E. Hertz, N.A. Papadogiannis, G. Nersisyan, C. Kalpouzos, T. Halfmann, D. Charalambidis, and G.D. Tsakiris, Phys. Rev. A **64**, 051801 (2001).

[17] M. Hentschel, R. Kienberger, Ch. Spielmann, G.A. Reider, N. Milosevic, T. Brabec, P. Corkum, U. Heinzmann, M. Drescher, and F. Krausz, Nature (London) **414**, 509 (2001).

[18] D. Kim, C. Toth, and C.P.J. Barty, Phys. Rev. A **59**, R4129 (1999); D. Kim, S.H. Son, J.H. Kim, C. Toth, and C.P.J. Barty, *ibid.* **63**, 023806 (2001).

[19] P. Sprangle, A. Ting, E. Esarey, and A. Fisher, J. Appl. Phys. **72**, 5032 (1992).

[20] E. Esarey, S.K. Ride, and P. Sprangle, Phys. Rev. E **48**, 3003 (1993).

[21] F.V. Hartemann, Phys. Plasmas **5**, 2037 (1998).

[22] T. Vachaspati, Phys. Rev. **128**, 664 (1962).

[23] L.S. Brown and T.W.B. Kibble, Phys. Rev. **133**, A705 (1964).

[24] E.S. Sarachik and G.T. Schappert, Phys. Rev. D **1**, 2738 (1970).

[25] Wei Yu, M.Y. Yu, J.X. Ma, and Z. Xu, Phys. Plasmas **5**, 406 (1998).

[26] S.-Y. Chen, A. Maksimchuk, and D. Umstadter, Nature (London) **396**, 653 (1998).

[27] S.-Y. Chen, A. Maksimchuk, E. Esarey, and D. Umstadter,

Phys. Rev. Lett. **84**, 5528 (2000).

[28] Y. Ueshima, Y. Kishimoto, A. Sasaki, and T. Tajima, Laser Part. Beams **17**, 45 (1999).

[29] A.E. Kaplan and P.L. Shkolnikov, Phys. Rev. Lett. **88**, 074801 (2002).

[30] J. D. Jackson, *Classical Electrodynamics*, 2nd ed. (Wiley, New York, 1975), Chap. 14.

[31] H. R. Griem, *Principles of Plasma Spectroscopy* (Cambridge University Press, Cambridge, 1997), p. 69.